IEEE Access
Multidisciplinary | Rapid Review | Open Access Journal

Received February 17, 2022, accepted February 28, 2022, date of publication March 8, 2022, date of current version March 18, 2022.

Digital Object Identifier 10.1109/ACCESS.2022.3157869

Surface Plasmon Polaritons in Time-Modulated Metallic Materials for Non-Reciprocal Controllable Leaky-Wave Antennas

MINH QUANG DINH AND MINH THUY LE, (Member, IEEE)
School of Electrical and Electronic Engineering, Hanoi University of Science and Technology, Hanoi 10999, Vietnam

Corresponding author: Minh Thuy Le (thuy.leminh@hust.edu.vn)

This work was supported in part by Vingroup Joint Stock Company (Vingroup JSC), Vingroup; and in part by the Vingroup Innovation Foundation (VINIF) under Project VINIF.2020.DA09.

ABSTRACT In this work, we propose using time-modulation in metallic materials, which can be realized through either optical pumps or electric signals, as a coupling mechanism between radiation and surface plasmon polaritons (SPP) without using any optical component. By applying temporal changes in the permittivity of metallic materials, scattered waves yield different frequencies from incident waves, potentially satisfying the continuous wave vector condition and enabling SPP from radiation. The coupling is observed in finite-difference time-domain simulations, where the dispersive metallic materials are modeled using auxiliary differential equations. Under the same modulation, coupling from radiation to SPP and from SPP to radiation differ strongly, showing clear evidence of the non-reciprocity. In addition, the coupling is also actively controllable via strength and frequency modulation. We also demonstrate the coupling at multiple angles, which is difficult to achieve with common methods such as Kretschmann or Otto configurations. The direct and non-reciprocal coupling between radiation and SPP can be beneficial for the application of telecommunication to form transmitting-only and receiving-only leaky-wave antennas in full-duplex transceivers.

INDEX TERMS Finite-difference time-domain, leaky waves, non-reciprocity, surface plasmon polariton, time-modulation.

I. INTRODUCTION

Surface plasmon polariton (SPP) is a special mode of electromagnetic wave that propagates at the interface between a metal and an insulator [1]. SPP can be formed in various ways but the most common one is from radiation. This coupling effectively turns the interface into an antenna which is a key component in communication. In addition, being highly directive and tightly confined at the interface [2], SPP decays exponentially in the direction normal to its propagating axis, offering a vast potential in communication in general and secured communication in particular.

Unfortunately, SPP cannot directly couple to radiation without intermediate optical components. In many cases, prisms are often used to create SPP. The main idea is to match the wave vector of SPP tangential to the interface with that of radiation, satisfying the boundary condition and facilitating the coupling between them. Such coupling schemes are referred to as Kretschmann [3] or Otto [4] configurations. Gratings can also be used as well [5]. However, optical components are not often available in the low-frequency regimes and thus different approaches have been developed. Notably, spatial modulation has been introduced as a way to couple free-space radiation and SPP [6], [7]. By introducing a phase-gradient in the SPP propagation direction, the requirement of the continuous-wave vector can be met, and thus SPP leaks out and radiates away. This method is, in fact, very similar to gratings since both aim to introduce an additional wave vector pertaining to the propagating medium to equalize those of radiation and SPP. Another way is to rely on the coupling between the SPP and coupled resonators [8]–[10]. Nevertheless, there is a common drawback in these traditional methods: it is difficult for most of them to be actively controlled, i.e., the coupling angle between radiation and SPP, the coupling efficiency, the frequency of radiation that can couple to SPP or vice versa cannot be actively tuned on a real-time basis.

The associate editor coordinating the review of this manuscript and approving it for publication was Pavlos I. Lazaridis.

Several earlier works have been dedicated to dealing with the real-time tunability of radiation-SPP coupling. For example, Wen *et al*. obtained the coupling efficiency tunability by using corrugated Ag-Al alloy electrode with the fixed periodicity and controlling with electric voltage [11]. The control of propagation directions of SPP, i.e., right-traveling or left-traveling, has been introduced by Lin *et al*. and You *et al*. by modulating the polarization of incident radiation [12], [13]. In addition, Liu *et al* proposed a structure that combined dielectric gratings, graphene, and electron beams that obtained coupling frequency tunability by controlling the bias voltage applied to graphene [14]. Another approach to controlling radiation-SPP coupling via controlling the instability of SPP in a structure of 2-D materials and bulk metals has also been theoretically studied [15]. In spite of the noteworthy accomplishments, the tunability of coupling angles has rarely been mentioned. For the application of SPP in communication, sometimes, the ''SPP antenna'' is required to transmit or receive from multiple angles and these angles must be controllable as well. This problem is also yet to be dealt with.

In addition to the difficulty in real-time control of coupling angles, there is another common trait in the proposed methods which is the Lorentz reciprocity. Although it is not categorized as a drawback, it is certainly not helpful in several applications of SPP, especially in communication. Due to this reciprocity, the coupling from SPP to radiation and vice versa are identical. The ''SPP antenna'' thus can both receive and transmit signals. The interference between these signals often poses a big problem, generating noises and distortion. Therefore, in communication applications, breaking the Lorentz reciprocity is desirable to create transmitting-only or receiving-only antennas, separating these signals.

To satisfy the above requirements of actively controlling the coupling angles and frequencies and breaking the Lorentz reciprocity in SPP-radiation coupling, we introduce time-modulation of the permittivity of metallic materials as an alternative approach to facilitate the coupling. Unlike those previously mentioned methods, it matches the wave vectors of radiation and SPP by causing a difference in their frequencies. Due to the modulation strength and frequency being variable, SPP can couple to radiation at different frequencies or angles of incidence. This is an effective solution to the tunability problem. Secondly, time-modulation may offer the very unique non-reciprocity [16], which means the coupling from SPP to radiation and from radiation to SPP/SSPP are not identical. With non-reciprocity, if SPP and radiation can couple to each other, strictly transmitting or strictly receiving antennas can be made. The result of this work, in particular, can be directly applied to make receiving-only or transmitting-only leaky-wave antennas, effectively solving the interference issue that we mentioned before. Recently, another approach to break the Lorentz-reciprocity for leaky-wave antennas based on topological photonics has been proposed [17]. Employing the topological photonic insulators, topological leaky-wave antennas only allow waves to travel in one direction. In the transmitted mode, waves go from a transmitting port to a radiating region and leak out. In the receiving mode, radiation is converted into guided waves and goes out to a receiving port. As a result, transmitted and received waves do not interfere since they occupy different areas. Therefore, a single topological antenna is able to both transmit and receive signals without having to worry about interference. This is a key difference compared to the time-modulated leaky-wave antennas which will be investigated. Another key advantage of topological antennas is that they are very robust to fabrication errors while time-modulated antennas are not, as we shall see in the following sections. However, time-modulated leaky-wave antennas also possess a distinct feature. As will be shown in the next section, since the coupling angle between SPP and radiation depends on the modulation frequency, by controlling it, we can easily tune the coupling angle on a real-time basis.

The contents of this paper are arranged as follows: Section II provides the theoretical analysis; section III provides the FDTD simulation set-up and simulation results in several scenarios; the conclusion is given in section IV.

II. THEORETICAL ANALYSIS

A. COUPLING BY TIME-MODULATION

We first begin with the theoretical analysis. The frequency-dependent permittivity ε_m of a metallic material at very high frequencies compared to its scattering rate is usually represented by the Drude model as:

$$\varepsilon_m(f) = 1 - \frac{f_p^2}{f^2} \tag{1}$$

where f is the frequency of waves in general and f_p is the plasma frequency. Below that plasma frequency, ε_m yields a negative value and the medium behaves like a metal. For SPP propagating on its interface with a dielectric ε_d with frequency f_{SPP}, the wave vector k_{SPP} takes the following form [18]:

$$k_{SPP} = \frac{2\pi f_{SPP}}{c_0}\sqrt{\frac{\varepsilon_m\varepsilon_d}{\varepsilon_m + \varepsilon_d}} \tag{2}$$

where c_0 is the light velocity in free-space. Radiation of frequency f_{rad} and amplitude H_{in} travelling from the dielectric medium to the interface has a wave vector of $k_{rad} = 2\pi f_{rad}\sqrt{\varepsilon_d}/c_0$. Radiation and SPP can couple if the part of their wave vectors tangential to the interface equal each other. The coupling condition is thus expressed as:

$$\frac{2\pi f_{SPP}}{c_0}\sqrt{\frac{\varepsilon_m\varepsilon_d}{\varepsilon_m + \varepsilon_d}} = \frac{2\pi f_{rad}\sqrt{\varepsilon_d}}{c_0} sin\theta \tag{3}$$

where θ is the angle of incidence. Normally, without any temporal perturbation, f_{SPP} equals f_{rad}. And because ε_m is negative, the above condition cannot be satisfied. With periodic time-modulation, ε_m varies periodically in time, making the frequencies different from each other. In particular, because ε_m is now periodic with frequency f_m, the impedance of the time-modulated metal $Z_m = \sqrt{\frac{\mu_0}{\varepsilon_0\varepsilon_m}}$ is also periodic, with the

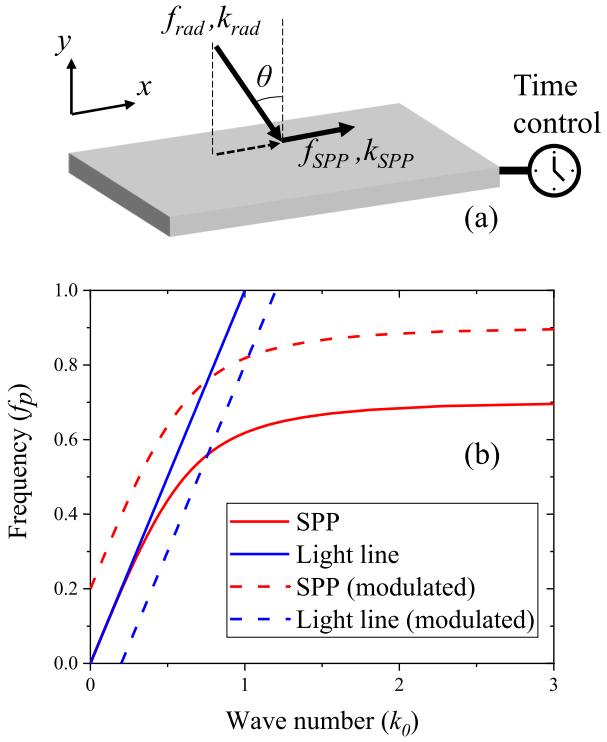

FIGURE 1. (a) Direct coupling mechanism between radiation and SPP by time-modulation in metallic materials. (b) Dispersion curves of SPP and radiation (light line) in the non-modulated (solid curves), SPP-to-radiation (red dash curve), and radiation to SPP (blue dash line).

same frequency f_m. The reflection coefficient $\Gamma = \frac{Z_0 - Z_m}{Z_0 + Z_m}$ is therefore also periodic, where $Z_0 = 120\pi\ \Omega$ is the free-space impedance. In the time domain, we have the following relation between the magnetic H field of the incident wave which is radiation, and the output wave which is either reflected radiation or SPP:

$$H_{out}(t) = \Gamma(t) H_{in}(t) \tag{4}$$

Since Γ is periodic, we can express its spectrum as follow:

$$\Gamma(f) = \Sigma_n \Gamma^n(f)\delta(f - nf_m) \tag{5}$$

Performing Fourier transform on equation (4), we obtain:

$$H_{out}(f) = \Sigma_n \Gamma^n(f_{rad}) H_{in}\delta(f - f_{rad} + nf_m) \tag{6}$$

From equation (6), we see that intermodulations (or harmonics) are added to the original frequency, and therefore, the output wave's frequency is:

$$f = f_{rad} + nf_m \tag{7}$$

where n is an integer called intermodulation index [19], [20]. Thus the wave vectors of incident and output waves can be matched and the output wave will be SPP if the following relation is true:

$$\frac{f_{SPP}}{f_{rad}} = \frac{f_{rad} + nf_m}{f_{rad}} = \sqrt{\frac{\varepsilon_m + \varepsilon_d}{\varepsilon_m}} sin\theta \tag{8}$$

Solving this equation, we may deduce the suitable modulation frequency f_m for the coupling to happen. From the above equations, it is obvious that SPP can only appear if ε_m is smaller than $-\varepsilon_d$. Thus the highest allowed frequency of SPP is $f_{SPPmax} = \frac{f_p}{\sqrt{(1+\varepsilon_d)}}$. Also, equation (8) can only be satisfied if f_{SPP} is smaller than f_{rad}. Therefore, f_m must takes certain values that after modulation, the remaining frequency $f_{SPP} = f_{rad}$-nf_m ($n \geq 1$) is lower than f_{SPPmax}. Note that only TM-polarized radiation can couple to SPP while TE-polarized radiation cannot. From here on, we will use the terms f_{SPP} for the SPP frequency, f_{rad} for the radiation frequency, f_p for the plasma frequency, and θ for the angle of incidence/departure.

B. NON-RECIPROCITY IN TIME-MODULATION-BASED COUPLING

The non-reciprocity can also be spotted in the above equations. If the metal's permittivity is engineered properly, the spectrum of Γ is dominated by only one value of intermodulation index n_1, we have:

$$\Gamma(f) = \Gamma^{n_1}(f)\delta(f - n_1 f_m) \tag{9}$$

Then both radiation and SPP that impinge on the time-modulated medium will experience a similar frequency shift of $n_1 f_m$. Because a downward shift is needed for radiation-to-SPP coupling and an upward shift is needed for the opposite coupling, only one of them can occur. The coupling process can therefore be non-reciprocal.

The coupling is illustrated in Fig. 1a. Fig. 1b shows the dispersions of SPP and radiation in the non-modulation, SPP-to-radiation coupling, and radiation-to-SPP coupling cases. Without modulation, the dispersion curve of SPP is always below the light line and thus no coupling may occur. To convert radiation to SPP, a decrease in frequency is needed, which corresponds to the light line being shifted to the left. For SPP-to-radiation coupling, an increase in frequency is needed, which corresponds to the dispersion curve of SPP being shifted upward. Coupling may occur at frequencies where the SPP dispersion is above the light line.

III. FDTD SIMULATION AND DISCUSSION

A. FDTD SIMULATION SET-UP

To validate the theoretical analysis, we build a 2-D FDTD simulation program in MATLAB using auxiliary differential equations [21], [22] with some modifications to match with the dispersive property of metallic materials. For TM-polarized waves, we let the magnetic field polarized in the z-axis and the electric field polarized in the x and y axes. The detailed simulation procedure and formulation can be found in Appendix.

For simplicity, we let the plasma frequency fluctuate around a central value following a sinusoidal rule:

$$f_p(t) = f_{p0} + \Delta sin(2\pi f_m t) \tag{10}$$

where Δ is the modulation strength and f_{p0} is the static plasma frequency. The modulation strength will determine

how much power from radiation is converted into SPP. Intuitively, a higher modulation strength will result in more radiation power being coupled to SPP and vice versa. However, it cannot be arbitrarily high because f_p must remain higher than radiation frequency f_{rad} all the time, otherwise, the metal will behave like a dielectric do not support the formation of SPP. The dielectric environment is formulated to be free-space with relative permittivity and permeability are all one. The surrounding boundaries are all perfectly matched layers. The 2-D simulation domain is divided into square meshes with the size of 0.025 c_0/f_{rad} x 0.025 c_0/f_{rad} and the time step is set as $\Delta t = \frac{S}{c_0\sqrt{\frac{1}{\Delta x^2}+\frac{1}{\Delta y^2}}}$, where Δx and Δy are the dimensions of the meshes, $S = 0.4$ is a coefficient added to further ensure the Courant – Friedrichs – Lewy condition for stability and make the results as accurate as possible. The entire simulation time is set as 40000 iterations, which is long enough to observe a stable phenomenon and also long enough to obtain accurate results from Fourier transform (if used). We performed simulations with f_{rad} equal 0.3 THz. However, the method can apply to any metal or doped semiconductor of any plasma frequency. Therefore, in the following sections, we will write all physical quantities as symbols instead of giving them specific values.

B. CASE-BY-CASE SIMULATIONS: NON-RECIPROCAL LEAKY-WAVE ANTENNAS FROM TIME-MODULATED METALLIC MATERIALS

In our simulation, the static plasma frequency f_{p0} is set as $1.05f_{rad}$, modulation strength Δ is 0.035. TM-polarized plane wave source that excites incident radiation is created according to the following rule:

$$H_{zsource} = H_0 sin(2\pi f_{rad} t + (x - x_0) sin\theta/\lambda) \qquad (11)$$

where x_0, x_{max} are two edges of the source, $x_0 < x < x_{max}$, λ is the wavelength in free-space. The angle of incidence is set as $\theta = 50°$. According to the previous analysis, in order to generate SPP, modulation frequency f_m should be around $0.445f_{rad}$. At one point on the interface where $x = 40c_0/f_{rad}$, we record the magnetic field strength then perform Fourier transform to find the SPP frequency (if there is any). Fig. 2(a) shows the simulation result with modulation frequency f_m equals $0.445f_{rad}$, with H-field intensity being normalized and 0 dB corresponding to the H-field intensity generated by the source. It is visible that from oblique incidence, SPP appears and travels at the interface. The H-field intensity of this SPP reaches up to -9 dB at several positions. When this frequency differs significantly from the calculated value, SPP does not appear as shown in Fig. 2(b) where f_m is $0.55f_{rad}$. We also change the modulation frequency to several other values far from $0.445f_{rad}$ and still observe the same outcome.

Fig. 3 shows the normalized spectrum analysis of signals at the interface for several cases in which radiation couples to SPP. As expected, the frequency f_{SPP} of recorded signals is always f_{rad}-f_m, smaller than the SPP cut-off frequency f_{SPPmax}, and all of them satisfy equation (8). From the above

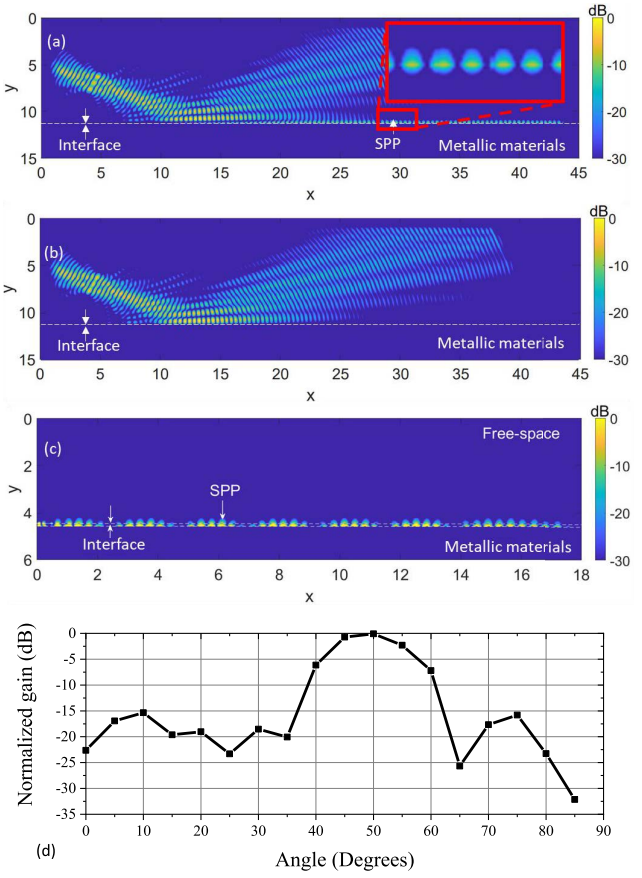

FIGURE 2. 2-D simulation results of H-field when radiation meets the dielectric-metal interface with $\theta = 50°$, $f_{p0} = 1.05f_{rad}$, $f_m = 0.445f_{rad}$ (a) and $f_m = 0.55f_{rad}$ (b). The interface is located at $y = 11.25\ c_0/f_{rad}$. (c) 2-D simulation result of H-field when SPP propagates on a time-modulated metal-dielectric interface, $f_{p0} = 1.89f_{SPP} = 1.05f_{rad}$, $f_m = 0.8f_{SPP} = 0.445f_{rad}$. The unit of both x and y is c_0/f_{rad}. (d) Normalized radiation pattern of the metallic surface in (a), (c).

simulation results, it is safe to say that the presented mechanism and theoretical analysis are plausible.

It should be noted that in this setting, one part of the incident radiation has its frequency down-converted by the time-modulated surface and turns into SPP while the rest has its frequency unchanged and is reflected back at the speculated direction. There is virtually no upward conversion in frequency. If there was any, we would have spotted an anomalous reflection at a narrower angle compared to the specular reflection. This implies a non-reciprocity in the coupling between SPP and radiation since an increase in frequency is needed to turn SPP into radiation. From Fig. 2(a), we can see the non-reciprocity quite clearly. While radiation is strongly coupled to SPP, the coupling from SPP to radiation is very weak. Because of that, SPP is able to propagate a long distance on the interface. If non-reciprocity did not exist, SPP would have been converted back into radiation right away because the medium in which it was traveling was being time-modulated. To confirm the non-reciprocity, we run another set of simulations, in which the condition is identical to previous

simulations with $f_{p0} = 1.05f_{rad}$ and $\Delta = 0.035$. We created an SPP source and observe whether there is any radiation leaking out. This SPP source has the following formulation:

$$H_{zsource} = H_0 e^{\alpha(y-y_m)+i2\pi f_{SPP}t} \tag{12}$$

where α is the decay coefficient in the y-axis, y_m is the position of the dielectric-metal interface. In free-space, α is $\frac{2\pi f}{c_0}\sqrt{\frac{1}{|1+\varepsilon_m|}}$ while in metal, it is $-\frac{2\pi f}{c_0}\sqrt{\frac{\varepsilon_m^2}{|1+\varepsilon_m|}}$ [1]. For $x < x_m = 5c_0/f_{rad}$, the metal is not modulated. From $x = x_m$, the metal is time-modulated following equation (10). Simulations are carried out several different cases, one of which has $f_m = 0.8f_{SPP}$ and $f_{p0} = 1.89f_{SPP}$, reciprocal to the simulation set-up of Fig. 2(a). Note that the values of f_{p0} all equal $1.05f_{rad}$, assuming $f_{rad} = f_{SPP} + f_m$ after modulation. According to equation (8), if radiation appears, it should depart at the angle of 50°. However, as seen from Fig. 2(c), radiation is absent (we only show the case when $f_m = 0.8f_{rad}$, the other case yields a similar outcome). The non-reciprocity is therefore confirmed. The time-modulated metallic material in this case behaves like a receiving-only leaky-wave antenna. The normalized radiation pattern of this antenna is shown in Fig. 2d. Due to symmetry, we only show the normalized gain corresponding to incident angles from 0° to 85°, the angles from −85° to 0° are similar. The cases of extreme incident angles ±90° are not calculated since at those angles, radiation and SPP propagate in parallel and thus they are difficult to tell apart. The main lobe is at 50°, the half-power beam width (HPBW) is about 10°, and the side lobes are lower than −15 dB.

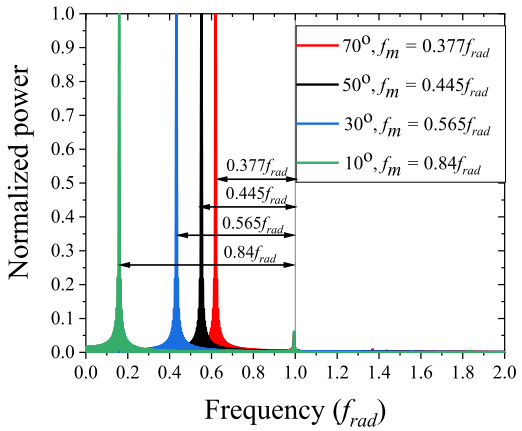

FIGURE 3. Normalized H-field amplitude spectrum of waves at the interfaces in four different cases with $f_{p0} = 1.05f_{rad}$.

After validating the theoretical analysis, we demonstrate a different case in which coupling from SPP to radiation occurs strongly while the opposite way is very weak. This time, we let $f_m = 0.45f_{SPP} = 0.31f_{rad}$, $f_{p0} = 2.5f_{SPP} = 1.72f_{rad}$. We hypothetically apply a very strong modulation signal with $\Delta = 0.4$. This modulation strength is just enough for f_p to be greater or equal to f_{rad} and f_{SPP} to be smaller than f_{SPPmax}. As shown in Fig. 4(a), after entering the modulated region,

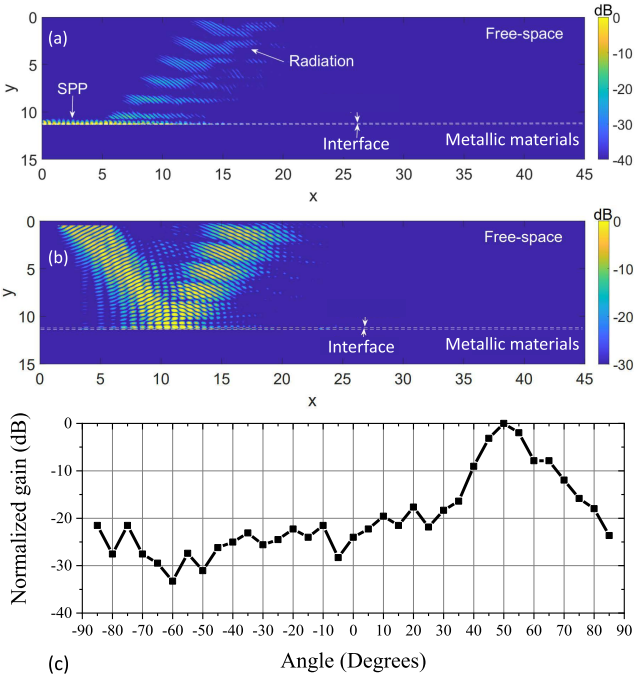

FIGURE 4. 2-D simulation result of H-field when only SPP-to-radiation coupling occurs, $f_m = 0.4f_{SPP} = 0.31f_{rad}$, $\Delta = 0.4$, $f_{p0} = 2.5f_{SPP} = 1.72f_{rad}$, incident/depart angle $\theta = 50°$. In the radiation-to-SPP coupling, SPP will leak back into free-space shortly after it appears. The unit of both x and y is c_0/f_{rad}. (c) Normalized radiation pattern of the metallic surface in (a), (b).

starting at $x_m = 5c_0/f_{rad}$, SPP begins to leak away from a 50° angle which is agreeable with equation (8). The remaining part travels another distance on the interface before being completely transformed into radiation. In the opposite way, radiation couples to SPP very weakly, as shown in Fig. 4(b). This is as expected since the modulation mostly increases the frequency. And even if coupling occurs, the portion of radiation converted to SPP also leaks back very quickly after traveling a short distance. Therefore, in this case, either the SPP does not appear or is short-lived, the metallic material behaves like a transmitting-only leaky-wave antenna. The normalized radiation pattern of this antenna is shown in Fig. 4c. Quite similar to the receiving-only case, the main lobe resides at 50°, the HPBW is about 10°, and the side lobes are lower than −17 dB.

From the presented simulations, we are certain that time-modulation of metallic materials may produce both radiation-to-SPP and SPP-to-radiation coupling. These couplings are non-reciprocal, and in addition to having a modulation frequency that satisfies equation (8), the modulation strength must be appropriate for a certain coupling to occur. From a photonic point of view, the energy of electromagnetic waves or light depends on frequency. An increase in frequency, which is needed for SPP-to-radiation coupling, will require more energy from the modulation source (i.e. the optical pumps). Therefore, the modulation has to be strong. In contrast, a decrease in frequency for radiation-to-SPP coupling

does not increase the energy of waves and thus can be realized with a weaker modulation strength. That explains why for small modulation ($\Delta = 0.035$), SPP does not leak out and turn into radiation while for strong modulation ($\Delta = 0.4$), SPP can couple to radiation. Radiation-to-SPP coupling will happen if the static plasma frequency is slightly higher than the radiation frequency and the modulation is weak. Meanwhile, SPP-to-radiation coupling happens if the static plasma frequency is much higher than the resulted radiation frequency and the modulation is strong.

Finally, after confirming the theory, finding out how to facilitate each coupling, and examining their non-reciprocity, we demonstrate a scenario in which the coupling occurs at multiple directions and the angle of each radiating/incident beam is controllable. By applying a multitone modulation signal consisting of two frequencies or more, the original frequency is converted into multiple bands, SPP leaks out and forms multiple radiation beams. Meanwhile, radiation from multiple angles of incidence can couple to the same surface. This is another distinct advantage of time-modulation compared to other common methods. In particular, for spatial modulation or Otto and Kretschmann configurations, there is only one value of incident angle to satisfy the wave-vector matching condition. Only gratings can couple SPP and radiation from multiple angles because it generates spatial harmonics. However, it is not actively controllable. Fig. 5(a) demonstrates this multi-directional coupling from SPP to radiation, in which the plasma frequency is $f_{p0} = 2.5f_{SPP}$, the two modulation frequencies are $f_{m1} = 0.7f_{SPP}$ and $f_{m2} = 0.15f_{SPP}$, two corresponding modulation strengths are $\Delta_1 = 0.35$ and $\Delta_2 = 0.2$. Fig. 5(b) and 5(c) demonstrate the multi-directional coupling from radiation to SPP at the angles of 40° and 60°, respectively, with similar settings: $f_{p0} = 1.3f_{rad}$, $f_{m1} = 0.315f_{rad}$ and $f_{m2} = 0.44f_{rad}$, $\Delta_1 = \Delta_2 = 0.1$. These frequencies and angles all satisfy equation (8) and radiation couples to SPP for both angles. The radiation patterns of the antennas are shown in Fig. 5d, e. In the transmitting-only case, two main lobes at the two frequencies $f_{rad1} = f_{SPP} + f_{m1}$ and $f_{rad2} = f_{SPP} + f_{m2}$ resides at 75° and 50°, with the latter is 4 dB-stronger than the former. For f_{rad2}, a side lobe at 65° is about −12 dB while other side lobes are lower than −18 dB. For f_{rad1}, all side lobes are lower than −16 dB. Both HPBWs are about 10° or narrower. For the receiving-only case, two main lobes corresponding to $f_{SPP1} = f_{rad} - f_{m1}$ and $f_{SPP2} = f_{rad} - f_{m2}$ are at 40° and 80°, with somewhat similar magnitude. Both HPBWs are also about 10° and all side lobes are lower than −16 dB.

We also examine the performance at different coupling angle by conducting two sets of simulations corresponding to two coupling directions, recording the H-field strength of SPP and radiation then performing Fourier transform to see the impacts of θ. The stronger H-field is the sight of the more efficient coupling and vice versa. For the radiation-to-SPP coupling simulations, the set-up is as follow: $f_{p0} = 1.05f_{rad}$, $\Delta = 0.035$ just like in Fig. 2, f_m is varied to change the coupling angle from 80° to 10°. The SPP H-field is recorded

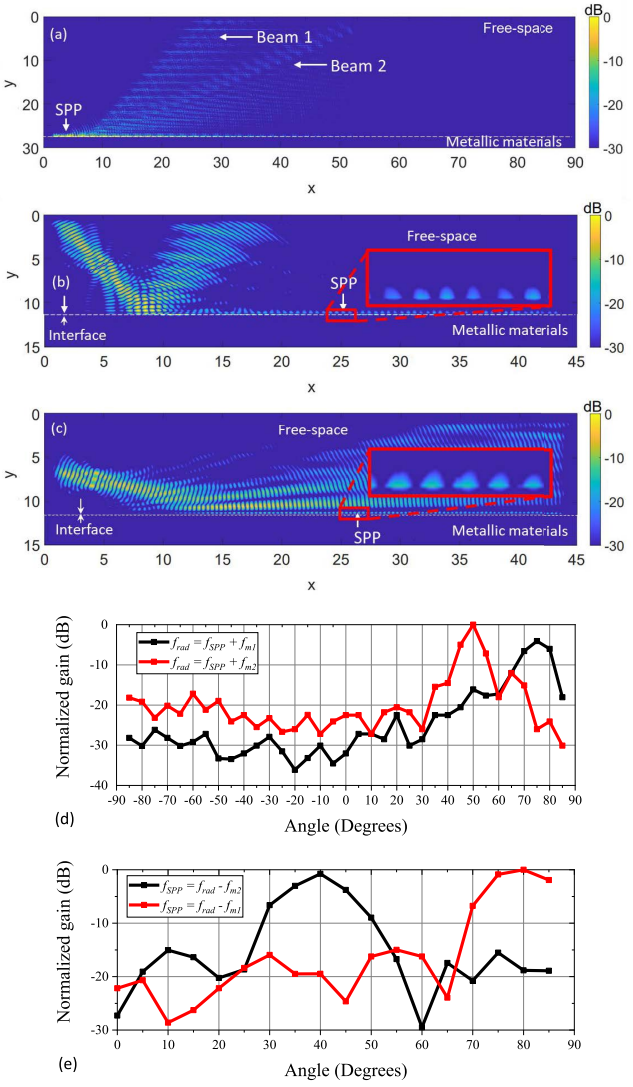

FIGURE 5. 2-D simulation result of H-field when coupling occurs at two angles: (a) SPP couples to two radiation beams, $f_{m1} = 0.4f$, $f_{m2} = 0.15f$, $\Delta f_{p1} = 0.35$, $\Delta f_{p2} = 0.2$, $f_{p0} = 2.5f$; (b), (c) radiation from 40° (b) and 80° (c) can couple to SPP at the same surface, $f_{p0} = 1.3f'$, $f_{m1} = 0.4f'$, $f_{m2} = 0.2f'$, $\Delta f_{p1} = \Delta f_{p2} = 0.1$. The unit of both x and y is c_0/f'. (d) Normalized radiation pattern of the metallic surface in (a); (e) normalized radiation pattern of the metallic surface in (b), (c).

on the interface, at $x = 40c_0/f_{rad}$, $y = y_m$ just like in Fig. 3. For the SPP-to-radiation coupling simulations, we set $f_{p0} = 1.72(f_{SPP} + f_m) = 1.72f_{rad}$, assuming $f_{rad} = f + f_m$ after modulation, $\Delta = 0.4$ just like in Fig. 4, f_m is also varied to control the coupling angle. The radiation H-field is recorded at $x = x_m + 10\sin\theta\ (c_0/f_{rad})$, $y = y_m + 10\cos\theta\ (c_0/f_{rad})$. The results are displayed in Fig. 6. For both couplings, we all see an optimal angle around 60° at which the coupling is the most efficient. The coupling is weakened as the angle approaches 10° or 80°, and will likely to decrease even more as the angle reaches the limits of 0° and 90°. This behavior is very similar to common leaky-wave antennas where radiation at both the broadside and end-fire directions is also weak [24]. The weak coupling at very narrow angles for SPP-to-radiation

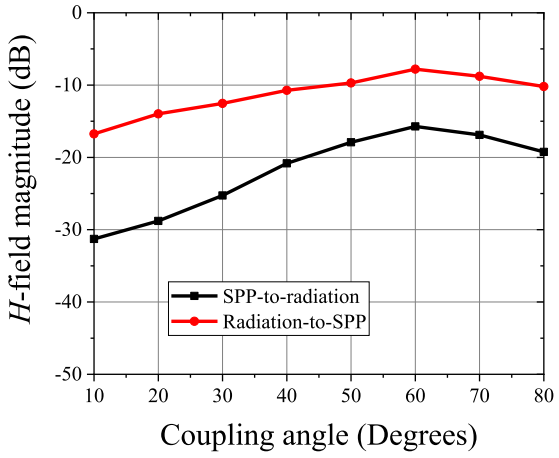

FIGURE 6. The impact of the angle of incidence/departure on both couplings. For the radiation-to-SPP coupling, $f_{p0} = 1.05f'$, $\Delta = 0.035$. For the SPP-to-radiation coupling, $f_{p0} = 1.72(f + f_m) = 1.72f'$, assuming $f' = f + f_m$ after modulation, $\Delta = 0.4$. Note that the H-field magnitude has been normalized in which 0 dB corresponds to the amplitude of the source. The strongest couplings occur around 60°.

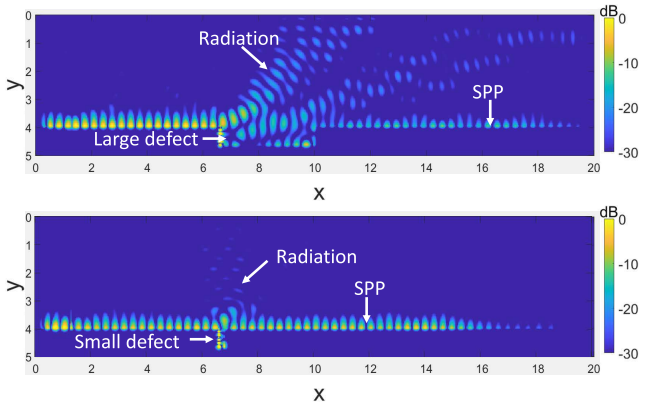

FIGURE 7. The impact of defect on the time-modulated SPP leaky-wave antennas. A significant part of SPP is converted into radiation with large defects (top) while for small defects, only a small part is radiated (bottom).

coupling can be interpreted as due to a very large frequency difference which approaches infinity as θ approaches 0° is needed. For radiation-to-SPP coupling, although the frequency difference needed is still finite, the resulting SPP frequency will approach 0 Hz at which ε_m approaches minus infinity and cannot support SPP. Meanwhile, for very wide angles, although in theory, only a small change in frequency is needed, the coupling is still weak. This can be explained as because SPP is TM wave, there is a longitudinal E-field that "flows" parallel to the interface along the propagation direction. And since free-space radiation is transverse electromagnetic (TEM) wave, this longitudinal E-field is what prohibits radiation at $\theta = 90°$.

For comparison purposes, we perform simulations of SPP propagation with defects and show the result in Fig. 7. It is clearly visible that unlike topological leaky-wave antennas, which are very robust [25], time-modulated leaky-wave antennas are still prone to defect or any other fabrication error. SPP will be scattered upon encountering obstacles. Part of it is converted into radiation and the size of the defect will determine how much power is radiated. This is a disadvantage of time-modulated leaky-wave antennas compared to their topological counterparts.

C. REALIZATION METHODS

There are several methods to realize time-modulation-based SPP-radiation coupling. Using ultrafast optical pumps is the first one of them, as shown in Fig. 8a. The metallic slab is modulated by external periodic optical pumps, which have been shown to have the ability to control the plasma frequency of general metals and other degenerately doped semiconductors [26], [27]. In fact, the work of Khurgin *et al*. has provided experimental proof for this possibility [28].

There are also several metallic materials in which permittivity can be actively tuned not with optical pumps but with electric signals. Graphene is one of them and several earlier works have investigated its tunability [29], [30]. We would like to emphasize that here we investigated the use of general metallic materials with time-modulation but before us, the works of Correas-Serrano *et al*. and Kashef *et al*. have particularly applied this concept for graphene, forming time-modulated leaky-wave antennas on graphene [31], [32]. This work seeks to further exploit and generalize that idea.

For graphene at the low THz which is close to its plasma frequency, its conductivity σ_g is dominated by the intraband component. Assuming the scattering rate is negligible compared to the considered frequency which is close to the plasma frequency, this conductivity is approximated as:

$$\sigma_g \approx \frac{e^2 E_F}{\pi h} \frac{i}{f} \tag{13}$$

where e is the electron charge, E_F is the Fermi energy level of graphene, and h represents the Planck constant. From this conductivity, one may express the frequency-dependent permittivity of graphene as:

$$\varepsilon_m = 1 + i\frac{\sigma_g}{2\pi f \varepsilon_0 d} = 1 - \frac{e^2 E_F}{2\pi^2 h \varepsilon_0 d f^2} \tag{14}$$

where d is the thickness of the graphene, which may vary from less than 1 nm with monolayer graphene to more with multilayer graphene. Here we see that the permittivity of graphene follows the Drude model as presented before and the plasma frequency is $f_{pg} = \sqrt{\frac{e^2 E_F}{2\pi^2 h \varepsilon_0 d}}$ which depends on E_F. Consider the case of a graphene sheet on top of an insulating layer with the permittivity ε_i, thickness d_i and backed by another conductor. A bias voltage V is applied to the graphene layer as shown in Fig. 8b. The Fermi energy of graphene, in this case, will depend on V according to the

following equation [29]:

$$E_F = \hbar v_F \sqrt{\frac{\pi \varepsilon_i V}{e d_i}} \tag{15}$$

where $\hbar$ is the reduced Planck constant and $v_F = 10^6$ is the Fermi velocity in graphene. From equations (14) and (15), we see that by applying a periodically varying voltage to graphene, its permittivity will be altered accordingly. Therefore time-modulation can be used on graphene to produce SPP from radiation and vice versa. Note that the above equations are all approximations. The plasma frequency of graphene, even at zero Fermi energy level, is still non-zero. In particular, in the commercial simulation software CST Microwave Studio, which supports the calculation of graphene permittivity and conductivity, one can find that it is around 16 THz. Also using CST Microwave Studio, we simulate a graphene sheet at a temperature of 293°K deposited on a 500-nm thick SiO_2 substrate. We observe that its plasma frequency varies from 16 THz to 38 THz, corresponding to $\Delta = 0.4$, as the Fermi energy goes from 0 eV to 0.16 eV, corresponding to a bias voltage of 0 V and 19 V (9.5 V-DC and 9.5 V-AC). However, with the current technology, we are not yet able to realize time-modulation coupling with graphene because it is uncommon for commercially available signal generators to create a 9.5 V-AC voltage at low-THz frequencies.

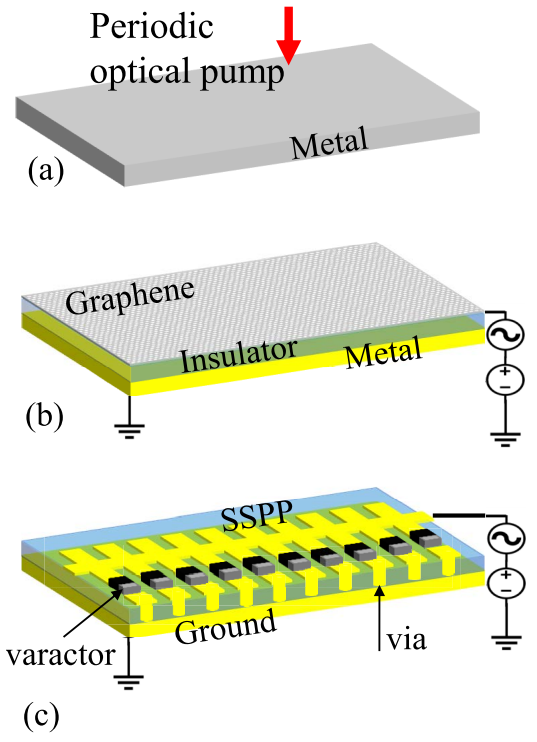

FIGURE 8. Direct coupling mechanism between radiation and SPP/SPP by time modulation via optical pumps (a) in general metallic materials, in graphene (b) and microwave SSPP transmission line (c) via electric signals.

Not only for metallic materials at high frequencies, time-modulation-based coupling can also be realized in the microwave region with SSPP using varactor diodes as tuning elements. For the microwave SSPP in the work of Zhang *et al*. [23], the cut-off frequency goes from 6 GHz to 9 GHz, corresponding to $\Delta = 0.2$, as the bias voltage goes from 0 V to 15 V, which is also realizable. The direct applications of this will be transmitting-only and receiving-only microwave antennas for radio-frequency communication. The configuration to facilitate coupling between radiation and SSPP is shown in Fig. 8c. Time-modulated devices and systems using varactors have been experimentally tested at several hundred MHz before [19], [33]. In [19], a time-modulated reflectarray unit cell using SMV1232 varactors achieves −7 dB reflection efficiency while the varactors are modulated at 600 MHz. In [33], a time-modulated patch antenna array using SMV1233 varactors achieves −4 dB efficiency while the varactors are modulated at 310 MHz. Therefore, we believe that time-modulated coupling can be realized with spoof SPP and varactors.

IV. CONCLUSION

In conclusion, we have studied time-modulation as a mechanism to couple radiation to SPP directly without using any optical component. By changing the permittivity of metallic materials periodically in time via optical pumps, a difference in frequency between incident radiation and SPP is created. Their wave vectors tangential to the interface can thus be matched, satisfying the continuous wave-vector condition and facilitating the coupling. The coupling has been observed in FDTD simulation. This coupling is non-reciprocal, with radiation being strongly coupled to SPP and SPP being weakly coupled to radiation or vice versa. Compared to other mechanisms, time-modulation offers a way to actively control the radiation and SPP coupling via tuning modulation frequency and strength. In addition, time-modulation can also facilitate coupling at multiple angles at the same condition. The non-reciprocity of the coupling mechanism is beneficial and can be relied on to create transmitting-only and receiving-only leaky-wave antennas, separating transmitted and received signals in full-duplex transceivers and other full-duplex systems.

APPENDIX A
FDTD FORMULATION AND SIMULATION PROCEDURE

The permeability is assumed to be non-dispersive $\mu = \mu_0$. The total displacement field D inside the dispersive time-modulated metal is described as:

$$D_{x,y}(f) = \varepsilon_0 E_{x,y}(f) + P_{x,y}(f) \tag{16}$$

where $P_{x,y}(f)$ is the polarization density and is expressed as:

$$P_{x,y}(f) = -\varepsilon_0 \frac{f_p^2(t)}{f^2} E_{x,y}(f) \tag{17}$$

Because the above equation is in both frequency domain and time domain, a transform to bring it to the time domain is

needed. After transforming $P_{x,y}(f)$ into the time domain using inverse Fourier transform, we have:

$$\frac{\delta^2 P_{x,y}(t)}{\delta t^2} = 4\pi^2 \varepsilon_0 f_p^2(t) E_{x,y}(t) \tag{18}$$

Dividing the 2-D space into discrete square meshes and the simulation time into discrete time steps, we have the discrete form of the above equation, which is used for calculating the polarization density at a particular point $x = i, y = j$ in space, at the n-th time step:

$$P_{x,y}^n(i,j) = 2P_{x,y}^{n-1}(i,j) - P_{x,y}^{n-2}(i,j) - 4\pi^2 \Delta t^2 \varepsilon_0 (f_p^n)^2 E_{x,y}^n(i,j) \tag{19}$$

where Δt is the time step. The E, H, D fields can be calculated from each other using Maxwell's equations. To be simple, we let the dielectric environment be non-dispersive, the E and H fields inside it will be calculated as:

$$E_x^n(i,j) = E_x^{n-1}(i,j) - \frac{\Delta t}{\varepsilon_0 \varepsilon_d \Delta y}[H_z^n(i,j) - H_z^n(i,j-1)] \tag{20}$$

$$E_y^n(i,j) = E_y^{n-1}(i,j) - \frac{\Delta t}{\varepsilon_0 \varepsilon_d \Delta x}[H_z^n(i,j) - H_z^n(i-1,j)] \tag{21}$$

$$H_z^n(i,j) = H_z^{n-1}(i,j) - \frac{\Delta t}{\mu_0 \Delta x}[E_y^n(i+1,j) - E_y^n(i,j)] + \frac{\Delta t}{\mu_0 \Delta y}[E_x^n(i,j+1) - E_y^n(i,j)] \tag{22}$$

where Δx and Δy are the dimensions of each square mesh. Inside the dispersive metal, using macroscopic Maxwell's equation, we have:

$$D_x^n(i,j) = D_x^{n-1}(i,j) - \frac{\Delta t}{\Delta y}[H_z^n(i,j) - H_z^n(i,j-1)] \tag{23}$$

$$D_y^n(i,j) = D_y^{n-1}(i,j) - \frac{\Delta t}{\Delta x}[H_z^n(i,j) - H_z^n(i-1,j)] \tag{24}$$

While the H field in this metal can be calculated similarly as in dielectric, the E field inside the dispersive metal will be calculated as:

$$E_{x,y}^n(i,j) = \frac{D_{x,y}^n(i,j) - P_{x,y}^n(i,j)}{\varepsilon_0} \tag{25}$$

The simulation procedure is as follow: first we create the simulation domain, set the time-step, the grid size, and the boundary condition; then all fields are set to zeros; then a simulation loop is created and runs for 40000 iterations; within each iteration, we first update the plasma frequency, the P-fields, the E-field and H-field in the dielectric; after that, we update the source amplitude before calculating the D, B, then E, H fields in the modulated metallic material.

The normalized radiation patterns are plotted by first measuring the field amplitude at each iteration, then performing Fourier transform to find out the field amplitude in the frequency domain.

ACKNOWLEDGMENT

The authors would like to thank Prof. Nguyen Thanh Tung with the Vietnam Academy of Science and Technology for helpful discussions.

REFERENCES

[1] J. Zhang, L. Zhang, and W. Xu, "Surface plasmon polaritons: Physics and applications," *J. Phys. D, Appl. Phys.*, vol. 45, no. 11, Mar. 2012, Art. no. 113001.

[2] A. K. Sharma, R. Jha, and B. D. Gupta, "Fiber-optic sensors based on surface plasmon resonance: A comprehensive review," *IEEE Sensors J.*, vol. 7, no. 8, pp. 1118–1129, Aug. 2007.

[3] E. Kretschmann, "Radiative decay of nonradiative surface plasmons excited by light," *Z. Naturforsch*, vol. 23, no. 12, pp. 2135–2136, 1968.

[4] A. Otto, "Excitation of nonradiative surface plasma waves in silver by the method of frustrated total reflection," *Zeitschrift Phys.*, vol. 216, pp. 398–410, Aug. 1968.

[5] R. H. Ritchie, E. T. Arakawa, J. J. Cowan, and R. N. Hamm, "Surface-plasmon resonance effect in grating diffraction," *Phys. Rev. Lett.*, vol. 21, no. 22, pp. 1530–1533, Nov. 1968.

[6] G. S. Kong, H. F. Ma, B. G. Cai, and T. J. Cui, "Continuous leaky-wave scanning using periodically modulated spoof plasmonic waveguide," *Sci. Rep.*, vol. 6, no. 1, Sep. 2016, Art. no. 29600.

[7] J. J. Xu, H. C. Zhang, Q. Zhang, and T. J. Cui, "Efficient conversion of surface-plasmon-like modes to spatial radiated modes," *Appl. Phys. Lett.*, vol. 106, no. 2, Jan. 2015, Art. no. 021102.

[8] J. Y. Yin, J. Ren, Q. Zhang, H. C. Zhang, Y. Q. Liu, Y. B. Li, X. Wan, and T. J. Cui, "Frequency-controlled broad-angle beam scanning of patch array fed by spoof surface plasmon polaritons," *IEEE Trans. Antennas Propag.*, vol. 64, no. 12, pp. 5181–5189, Dec. 2016.

[9] J. Y. Yin, D. Bao, J. Ren, H. C. Zhang, B. C. Pan, Y. Fan, and T. J. Cui, "Endfire radiations of spoof surface plasmon polaritons," *IEEE Antennas Wireless Propag. Lett.*, vol. 16, pp. 597–600, 2017.

[10] Q. L. Zhang, B. J. Chen, K. F. Chan, and C. H. Chan, "Terahertz circularly- and linearly polarized leaky-wave antennas based on spin–orbit interaction of spoof surface plasmon polaritons," *IEEE Trans. Antennas Propag.*, vol. 69, no. 8, pp. 4347–4358, Aug. 2021.

[11] X. M. Wen, Y. G. Bi, F. S. Yi, X. L. Zhang, Y. F. Liu, W. Q. Wang, J. Feng, and H. B. Sun, "Tunable surface plasmon-polariton resonance in organic light-emitting devices based on corrugated alloy electrodes," *Opto-Electron. Adv.*, vol. 4, no. 8, 2021, Art. no. 200024.

[12] J. Lin, J. P. B. Mueller, Q. Wang, G. Yuan, N. Antoniou, X.-C. Yuan, and F. Capassor, "Polarization-controlled tunable directional coupling of surface plasmon polaritons," *Science*, vol. 340, pp. 331–334, Apr. 2013.

[13] O. You, B. Bai, L. Sun, B. Shen, and Z. Zhu, "Versatile and tunable surface plasmon polariton excitation over a broad bandwidth with a simple metaline by external polarization modulation," *Opt. Exp.*, vol. 24, pp. 22061–22073, Sep. 2016.

[14] S. Liu, C. Zhang, M. Hu, X. Chen, P. Zhang, S. Gong, T. Zhao, and R. Zhong, "Coherent and tunable terahertz radiation from graphene surface plasmon polaritons excited by an electron beam," *Appl. Phys. Lett.*, vol. 104, no. 20, May 2014, Art. no. 201104.

[15] G. Gumbs, A. Iurov, D. Huang, and W. Pan, "Tunable surface plasmon instability leading to emission of radiation," *J. Appl. Phys.*, vol. 118, no. 5, Aug. 2015, Art. no. 054303.

[16] A. Shaltout, A. Kildishev, and V. Shalaev, "Time-varying metasurfaces and Lorentz non-reciprocity," *Opt. Mater. Exp.*, vol. 5, no. 11, pp. 2459–2467, 2015.

[17] Z. Xu, M. Wang, S. Fang, H. Liu, Z. Wang, and D. F. Sievenpiper, "Broadside radiation from Chern photonic topological insulators," *IEEE Trans. Antennas Propag.*, vol. 70, no. 3, pp. 2358–2363, Mar. 2022, doi: 10.1109/TAP.2021.3111256.

[18] W. X. Tang, H. C. Zhang, H. F. Ma, W. X. Jiang, and T. J. Cui, "Concept, theory, design, and applications of spoof surface plasmon polaritons at microwave frequencies," *Adv. Opt. Mater.*, vol. 7, no. 1, Jan. 2019, Art. no. 1800421.

[19] J. W. Zang, D. Correas-Serrano, J. T. S. Do, X. Liu, A. Alvarez-Melcon, and J. S. Gomez-Diaz, "Nonreciprocal wavefront engineering with time-modulated gradient metasurfaces," *Phys. Rev. A, Gen. Phys.*, vol. 11, no. 5, May 2019, Art. no. 054054.

[20] D. Ramaccia, D. L. Sounas, A. Alu, A. Toscano, and F. Bilotti, "Phase-induced frequency conversion and Doppler effect with time-modulated metasurfaces," *IEEE Trans. Antennas Propag.*, vol. 68, no. 3, pp. 1607–1617, Mar. 2020.

[21] A. Taflove and S. C. Hagness, *Computational Electromagnetics: The Finite-Difference Time-Domain Method*. Boston, MA, USA: Artech House, 2005.

[22] A. Pekmezci and L. Sevgi, "FDTD-based metamaterial (MTM) modeling and simulation [testing ourselves]," *IEEE Antennas Propag. Mag.*, vol. 56, no. 5, pp. 289–303, Oct. 2014.
[23] H. C. Zhang, P. H. He, X. Gao, W. X. Tang, and T. J. Cui, "Pass-band reconfigurable spoof surface plasmon polaritons," *J. Phys., Condens. Matter*, vol. 30, no. 13, Apr. 2018, Art. no. 134004.
[24] F. Monticone and A. Alù, "Leaky-wave theory, techniques, and applications: From microwaves to visible frequencies," *Proc. IEEE*, vol. 103, no. 5, pp. 793–821, May 2015.
[25] Z. Xu, X. Kong, R. J. Davis, D. Bisharat, Y. Zhou, X. Yin, and D. F. Sievenpiper, "Topological valley transport under long-range deformations," *Phys. Rev. Res.*, vol. 2, no. 1, Feb. 2020, Art. no. 013209.
[26] O. Reshef, I. D. Leon, M. Z. Alam, and R. W. Boyd, "Nonlinear optical effects in epsilon-near-zero media," *Nature Rev. Mater.*, vol. 4, no. 8, pp. 535–551, Aug. 2019.
[27] Z. Hayran and F. Monticone, "Capturing broadband light in a compact bound state in the continuum," *ACS Photon.*, vol. 8, no. 3, pp. 813–823, Mar. 2021.
[28] J. B. Khurgin, M. Clerici, V. Bruno, L. Caspani, C. DeVault, J. Kim, A. Shaltout, A. Boltasseva, V. M. Shalaev, M. Ferrera, D. Faccio, and N. Kinsey, "Adiabatic frequency shifting in epsilon-near-zero materials: The role of group velocity," *Optica*, vol. 7, pp. 226–231, Mar. 2020.
[29] M. Q. Dinh, T. V. Huynh, B. X. Khuyen, B. S. Tung, V. D. Lam, S. T. Ngo, M. T. Le, and N. T. Tung, "Graphene-integrated hybridized metamaterials for wide-angle tunable THz absorbers," *Photon. Nanostruct. Fundam. Appl.*, vol. 45, Jul. 2021, Art. no. 100924.
[30] J. S. Gómez-Díaz and J. Perruisseau-Carrier, "Graphene-based plasmonic switches at near infrared frequencies," *Opt. Exp.*, vol. 21, no. 13, p. 15490, 2013.
[31] D. Correas-Serrano, J. S. Gómez-Díaz, D. Sounas, A. Alvarez-Melcon, and A. Alú, "Non-reciprocal graphene devices and antennas at THz based on spatio-temporal modulation," *IEEE Antennas Wireless Propag. Lett.*, vol. 15, pp. 1529–1533, 2016.
[32] M. M. Kashef and Z. G. Kashani, "Multifunctional space-time phase modulated graphene metasurface," *J. Opt. Soc. Amer. B, Opt. Phys.*, vol. 37, pp. 3243–3250, 2020.
[33] J. W. Zang, A. Alvarez-Melcon, and J. S. Gomez-Diaz, "Nonreciprocal phased-array antennas," *Phys. Rev. A, Gen. Phys.*, vol. 12, no. 5, Nov. 2019, Art. no. 054008.

MINH QUANG DINH received the Dip. (Eng.) degree in electrical engineering from the Hanoi University of Science and Technology, in 2021. He is currently working on photonics.

MINH THUY LE (Member, IEEE) was born in Vietnam. She received the B.E. and M.S. degrees in electrical engineering from the Hanoi University of Science and Technology (HUST), in 2006 and 2008, respectively, and the Ph.D. degree in optics and radio frequency from the Grenoble Institute of Technology, France, in 2013. She is currently a Lecturer and also a Group Leader of the Radio Frequency Group, Department of Instrumentation and Industrial Informatics (3I), School of Electrical Engineering (SEE), HUST. Her current research interests include built-in antenna, antenna array, beamforming, metamaterials, indoor localization and RF energy harvesting, wireless power transfer, and autonomous wireless sensor.